

Two-Stage Robust Optimal Operation of Distribution Networks using Confidence Level Based Distributionally Information Gap Decision

Zhisheng Xiong, *Graduate Student Member, IEEE*, Bo Zeng, *Member, IEEE*, Peter Palensky, *Senior Member, IEEE*, Pedro P. Vergara, *Senior Member, IEEE*.

Abstract—This paper presents a confidence level-based distributionally information gap decision theory (CL-DIGDT) framework for the two-stage robust optimal operation of distribution networks, aiming at deriving an optimal operational scheme capable of addressing uncertainties related to renewable energy and load demands. Building on conventional IGDT, the proposed framework utilizes the confidence level to capture the asymmetric characteristics of uncertainties and maximize the risk-averse capability of the solution in a probabilistic manner. To account for the probabilistic consideration, the imprecise Dirichlet model is employed to construct the ambiguity sets of uncertainties, reducing reliance on precise probability distributions. Consequently, a two-stage robust optimal operation model for distribution networks using CL-DIGDT is developed. An iterative method is proposed to solve the model and determine the upper and lower bounds of the objective function. Case study demonstrates that the proposed approach yields a more robust and statistically optimized solution with required accuracy compared to existing method, contributing to a reduction in first-stage cost by 0.84%, second-stage average cost by 6.7%, and significantly increasing the reliability of the solution by 8%.

Index Terms—Robust optimization, information gap decision theory, probability, ambiguity set, distribution networks.

NOMENCLATURE

A. Sets:

\mathcal{N}	Set of nodes of the distribution network
\mathcal{L}	Set of lines
\mathcal{G}	Set of nodes in which a DG unit is connected, $\mathcal{G} \subset \mathcal{N}$
\mathcal{B}	Set of nodes in which an ESS is connected, $\mathcal{B} \subset \mathcal{N}$
\mathcal{T}	Set of time-periods

B. Indexes:

ij	Line $ij \in \mathcal{L}$
i, j	Nodes $i \in \mathcal{N}$ and $j \in \mathcal{N}$
t	Time interval $t \in \mathcal{T}$

C. Parameters:

c_i, \hat{c}_i	First/Second-stage DGs operational cost
d_t, \hat{d}_t	First/Second-stage electricity purchase cost
$\bar{e}_{i,t}, \underline{e}_{i,t}$	Maximum/Minimum energy capacity of ESSs

$\bar{p}^{B+}, \underline{p}^{B+}$	Maximum/Minimum charging power of ESSs
$\bar{p}^{B-}, \underline{p}^{B-}$	Maximum/Minimum discharging power of ESSs
η_B	Efficiency of the ESSs
$\bar{p}_i^G, \underline{p}_i^G$	Maximum/Minimum active power of the DGs
$\bar{q}_i^G, \underline{q}_i^G$	Maximum/Minimum reactive power of the DGs
\bar{p}^l	Maximum power flow limit
\bar{v}, \underline{v}	Maximum/Minimum limit of $\hat{v}_{i,t}$
r_{ij}	Line resistance
x_{ij}	Line reactance
RU_i, RD_i	Ramp up/down limit of the DGs
$p^{PV,cap}$	Capacity of solar panels
Δt	Time step period
D. Continuous Variables:	
$e_{i,t}$	Energy of the ESSs
$\hat{p}_{i,t}^G$	Active output of the DGs after recourse action
\hat{p}_i^S, \hat{p}_i^D	First/Second-stage purchased power
$p_{ij,t}, \hat{p}_{ij,t}$	First/Second-stage active power flow
$q_{ij,t}, \hat{q}_{ij,t}$	First/Second-stage reactive power flow
$v_{i,t}, \hat{v}_{i,t}$	First/Second-stage square of bus voltage magnitude
$\delta_{i,t}$	Power factor angle

I. INTRODUCTION

DISTRIBUTION networks (DNs) are increasingly integrating high shares of renewable energy sources (RESs). The intermittent and volatile nature of RESs, along with the uncertainty in load demands, can affect both the economics and security of the networks [1]. For instance, failure to appropriately address uncertainty may increase operational costs due to actions such as load shedding, RESs curtailment, and the need for excessive reserves. Moreover, potential risks may incur, such as voltage violations and line overloading. These significant challenges to the optimal operation of DN may undermine the transition to more sustainable energy systems. Accordingly, numerous studies have been conducted to manage the uncertainties associated with RESs and load demands, aiming to develop robust operational strategies that enhance the cost-effectiveness and reliability of DN.

Most research on the optimal operation of DN under uncertainty relies on varying levels of information about the random

Zhisheng Xiong, Peter Palensky and Pedro P. Vergara are with the Intelligent Electrical Power Grids (IEPG) group, Delft University of Technology, 2628 CD Delft, Netherlands (e-mail: {z.xiong, p.palensky, p.p.vergarabarríos}@tudelft.nl).

Bo Zeng is with the Department of Industrial Engineering and the Department of Electrical and Computer Engineering, University of Pittsburgh, Pittsburgh, PA 15106 USA (e-mail: bzeng@pitt.edu).

variables: complete, partial, or none at all. Ref. [2] models the wind power loss and line overloading as chance constraints using a truncated normal distribution, establishing a two-stage stochastic programming (SP) model for unit commitment. Ref. [3] presents a two-stage stochastic dynamic economic dispatch model that effectively addresses wind power uncertainty. This model improves cost efficiency and reliability by pre-dispatching generator output to avoid network congestion in the first stage and re-dispatching resources after the realization of the wind scenarios. Ref. [4] incorporates multiple correlations of RESs through probability distributions (PDs) and scenario analysis into a multi-time scale SP framework. By managing slow- and fast-response resources to coordinate active and reactive power, the economical performance and the secure operation of the system are ensured under RESs uncertainty. SP features the need for PDs or uncertain scenarios, making its performance closely tied to the accuracy of PDs or the number of scenarios, which can be well guaranteed with an incredibly large amount of historical data.

Robust optimization (RO) uses the boundary information of uncertainties, making it a practical choice for the optimal operation of DNs. However, solutions derived from RO tend to be conservative because they focus solely on the worst-case scenario within a predefined uncertainty set, ignoring any information on the uncertainties. To mitigate the conservatism, Ref. [5] searches the extreme scenarios to redesign traditional uncertainty sets within a two-stage RO framework, yielding a less conservative yet robust solution for determining the tap ratio of transformers and the capacity of switching capacitors. Similarly, Ref. [6] reconstructs the uncertainty set of wind power based on historical data, aiming to reduce conservatism in economic dispatch. In addition to RO, distributionally robust optimization (DRO) incorporates partial information on uncertainties to minimize operational cost over the worst-case PD within ambiguity sets constructed from historical data. This approach leverages available information on uncertainties, thereby reducing conservatism. For instance, Ref. [7] introduces a moment-based DRO to characterize renewable generation uncertainty for real-time power dispatch in DNs. Ref. [8] constructs an ambiguity set of wind power using Wasserstein-based DRO, followed by a chance constraint-based DRO model for reactive power dispatch. In Ref. [9], the imprecise Dirichlet model (IDM) is used to construct the ambiguity set of wind power, with a conditional value at risk (CVaR) indicator to identify the worst-case distribution, aiming to balance operational costs and the risks of wind curtailment in real-time energy dispatch.

It is well-established that a larger uncertainty set (ambiguity set) increases robustness whereas reduces economic performance. Several critical challenges thus arise in the optimization process, such as the size of the predefined uncertainty set, the amount of operational cost budget allocated, as well as the trade-off between robustness and economic performance. Many of the aforementioned approaches fail to simultaneously address these challenges effectively. Information gap decision theory (IGDT) provides a robust decision-making framework for handling severe uncertainties without requiring any information or a predefined uncertainty set [10]. Risk-averse based-

IGDT seeks to optimize the uncertainty set within a preset financial budget, which is particularly useful when there is a clear target, such as a desired budget for the operation of DNs. For example, Ref. [11] models the uncertainty of load demand with limited data to provide a robust optimal decision for IGDT-based three-phase optimal power flow. To address frequency excursions resulting from load and RESs fluctuations, an IGDT-based energy management system is proposed for islanded microgrids in Ref. [12]. Ref. [13] utilizes IGDT to find a robust operation scheme against uncertainties in wind power, solar power, and load for resiliency-oriented DNs. The envelop-bound uncertainty modeling of IGDT has extensively applied in DNs operation [11]–[13], network planning [14], electricity market offering strategy [15], etc., due to its capability to handle forecasted types of uncertainty sources [10]. Despite the advantages of IGDT, its uncertainty modelling does not incorporate specific information on uncertainties, and the real-valued symmetric uncertainty sets limit the approach to capture the asymmetric characteristics of uncertainties. The asymmetry of uncertainties primarily refers to scenarios that deviate significantly from the expected scenarios but still have a relatively high probability of occurrence, such as those found in the heavy tails of PDs. These scenarios can have substantial impacts when they occur. However, many existing uncertainty modelling approaches fail to account for these significant scenarios probabilistically, or neglect to incorporate the desired operational cost budget when defining uncertainty sets. While SP considers the probability of scenarios, as previously discussed, its accuracy is highly dependent on the distribution type and the size of the dataset.

Base on the above discussion, we propose a novel uncertainty modelling approach that utilizes confidence level to capture the asymmetric characteristics of uncertain parameters and maximize risk-averse capability in a probabilistic manner within the IGDT framework, while adhering to a desired budget. The IDM is employed to construct the ambiguity sets, leveraging available data and mitigating the dependency on PDs. Consequently, the confidence level-based distributionally IGDT (CL-DIGDT) framework is developed for the two-stage robust optimal operation of DNs. An iterative method is proposed to solve the model and determine the upper and lower bounds of the objective function. Overall, the main contributions of this paper are as follows:

- A two-stage DNs optimal operation model is constructed using CL-DIGDT. In the proposed framework, the confidence interval replaces the real-valued symmetric interval of IGDT, which captures the asymmetric characteristics of the uncertainties associated with RESs and load demands. Additionally, the newly defined objective function ensures the robustness of the solution by describing better the risk-averse capability in a probabilistic way, compared with the traditional IGDT.
- IDM is utilized to construct the ambiguity sets for RESs and load demands, and integrated into the proposed optimization model. This method reduces reliance on precise PDs and leverages the available data at hand.
- To solve the integrated model, an iterative method is

employed to determine the upper and lower bounds of the objective function. The iterative process continues until the objective value converges to a specified accuracy, at which point the solution is deemed sufficiently precise.

II. MATHEMATICAL FORMULATION

The necessity for a two-stage operation model arises from the challenges of multi-time scale control in DNs [7]. Consequently, this section introduces an optimization model for DNs optimal operation problem, consisting of an economic dispatch plan and a recourse control stage. In the first stage, the approximate active power plan is scheduled based on expected uncertain scenarios. In the second stage, both active and reactive power regulation are implemented based on the real realization of uncertain scenarios, aiming to minimize resource costs and ensure system security. Two types of distributed energy resources are considered dispatchable: distributed generators (DGs) and energy storage systems (ESSs).

A. First-stage Economic Dispatch Plan

In the first stage, decisions regarding the active power of DGs ($p_{i,t}^G$) and the charging/discharging power of ESSs ($p_{i,t}^{B+}/p_{i,t}^{B-}$) are defined based on expected forecasts for renewable energy ($\tilde{p}_{i,t}^{PV}$) and load demands ($\tilde{p}_{i,t}^L$), to determine the approximate active power output plan.

1) *Objective function*: The operational costs (Λ_1) include the cost of active power output from the DGs and the cost of electricity purchased from the upstream main grid.

$$\min \Lambda_1 = \sum_{t \in \mathcal{T}} \left(\sum_{i \in \mathcal{G}} c_i p_{i,t}^G + d_t p_t^S \right) \quad (1)$$

2) *DGs constraints*: The DGs constraints are composed of the active output limits (2a), and the ramp up/down limits (2b)–(2c).

$$\underline{p}_i^G \leq p_{i,t}^G \leq \bar{p}_i^G, \forall i \in \mathcal{G}, \forall t \in \mathcal{T} \quad (2a)$$

$$p_{i,t}^G - p_{i,t-1}^G \leq RU_i, \forall i \in \mathcal{G}, \forall t \in \mathcal{T} \quad (2b)$$

$$p_{i,t-1}^G - p_{i,t}^G \leq RD_i, \forall i \in \mathcal{G}, \forall t \in \mathcal{T} \quad (2c)$$

3) *ESSs constraints*: The ESSs constraints include the energy storage capacity (3a), the capacity limits (3b), and the charging/discharging limits (3c)–(3d).

$$e_{i,t} = e_{i,t-1} + \eta_B p_{i,t}^{B+} \Delta t - \frac{p_{i,t}^{B-}}{\eta_B} \Delta t, \forall i \in \mathcal{B}, \forall t \in \mathcal{T} \quad (3a)$$

$$e_i \leq e_{i,t} \leq \bar{e}_i, \forall i \in \mathcal{B}, \forall t \in \mathcal{T} \quad (3b)$$

$$z_{i,t} p_{i,t}^{B+} \leq p_{i,t}^{B+} \leq z_{i,t} \bar{p}^{B+}, \forall i \in \mathcal{B}, \forall t \in \mathcal{T} \quad (3c)$$

$$(1 - z_{i,t}) \underline{p}^{B-} \leq p_{i,t}^{B-} \leq (1 - z_{i,t}) \bar{p}^{B-}, \forall i \in \mathcal{B}, \forall t \in \mathcal{T} \quad (3d)$$

where $z_{i,t}$ is the binary variable that models the operational mode of ESSs, with $z_{i,t} = 1$ indicating the charging mode and $z_{i,t} = 0$ the discharging mode.

4) *Power flow constraints*: Constraints (4a) model the active power balance equations, and constraints (4b) consider the net active loads ($p_{i,t}$).

$$\sum_{hi \in \mathcal{L}} p_{hi,t} - \sum_{ij \in \mathcal{L}} p_{ij,t} = p_{i,t}, \forall i \in \mathcal{N}, \forall t \in \mathcal{T} \quad (4a)$$

$$p_{i,t} = p_{i,t}^G + p_{i,t}^{B+} - p_{i,t}^{B-} + \tilde{p}_{i,t}^{PV} - \tilde{p}_{i,t}^L, \forall i \in \mathcal{N}, \forall t \in \mathcal{T} \quad (4b)$$

5) *Network security constraints*: The maximum power flow limits are enforced by constraints (5).

$$-\bar{p}^l \leq p_{ij,t} \leq \bar{p}^l, \forall ij \in \mathcal{L}, \forall t \in \mathcal{T} \quad (5)$$

B. Second-stage Recourse Control Stage

Decisions on the recourse actions involving the active and reactive power outputs of DGs ($\hat{p}_{i,t}^G/\hat{q}_{i,t}^G$) are defined based on the real realizations of renewable energy ($p_{i,t}^{PV}$) and load demands ($p_{i,t}^L$), to guarantee the minimal recourse control cost and the system security. The proposed model aims to enhance operational flexibility and coordination, ensuring a less-conservative strategy under actual operating conditions.

1) *Objective function*: The recourse control cost (Λ_2) is determined by the cost of recourse active power output of the DGs and the cost of additional electricity purchased from the main grid.

$$\min \Lambda_2 = \sum_{t \in \mathcal{T}} \left(\sum_{i \in \mathcal{G}} \hat{c}_i \hat{p}_{i,t}^G + \hat{d}_t (\hat{p}_t^S - p_t^S) \right) \quad (6)$$

2) *DGs recourse constraints*: The DGs constraints are composed of the recourse capability limits (7a), the reactive output limits (7b), the active output after recourse control (7c) as well as the ramp up/down limits of the active output after recourse control (7d)–(7e).

$$\underline{\hat{p}}_i^G \leq \hat{p}_{i,t}^G \leq \bar{\hat{p}}_i^G, \forall i \in \mathcal{G}, \forall t \in \mathcal{T} \quad (7a)$$

$$\underline{\hat{q}}_i^G \leq \hat{q}_{i,t}^G \leq \bar{\hat{q}}_i^G, \forall i \in \mathcal{G}, \forall t \in \mathcal{T} \quad (7b)$$

$$\hat{p}_{i,t}^G = p_{i,t}^G + \hat{p}_{i,t}^G, \forall i \in \mathcal{G}, \forall t \in \mathcal{T} \quad (7c)$$

$$\hat{p}_{i,t}^G - \hat{p}_{i,t-1}^G \leq RU_i, \forall i \in \mathcal{G}, \forall t \in \mathcal{T} \quad (7d)$$

$$\hat{p}_{i,t-1}^G - \hat{p}_{i,t}^G \leq RD_i, \forall i \in \mathcal{G}, \forall t \in \mathcal{T} \quad (7e)$$

3) *Power flow and voltage constraints*: Constraints (8a)–(8b) model the active/reactive power balance equations. Constraints (8c)–(8e) consider the net active/reactive loads ($\hat{p}_{i,t}/\hat{q}_{i,t}$), and (8f) is the voltage magnitude drop in the lines.

$$\sum_{hi \in \mathcal{L}} \hat{p}_{hi,t} - \sum_{ij \in \mathcal{L}} \hat{p}_{ij,t} = \hat{p}_{i,t}, \forall i \in \mathcal{N}, \forall t \in \mathcal{T} \quad (8a)$$

$$\sum_{hi \in \mathcal{L}} \hat{q}_{hi,t} - \sum_{ij \in \mathcal{L}} \hat{q}_{ij,t} = \hat{q}_{i,t}, \forall i \in \mathcal{N}, \forall t \in \mathcal{T} \quad (8b)$$

$$\hat{p}_{i,t} = \hat{p}_{i,t}^G + p_{i,t}^{B+} - p_{i,t}^{B-} + p_{i,t}^{PV} - p_{i,t}^L, \forall i \in \mathcal{N}, \forall t \in \mathcal{T} \quad (8c)$$

$$\hat{q}_{i,t} = \hat{q}_{i,t}^G - q_{i,t}^L, \forall i \in \mathcal{N}, \forall t \in \mathcal{T} \quad (8d)$$

$$q_{i,t}^L = p_{i,t}^L \tan \delta_{i,t}, \forall i \in \mathcal{N}, \forall t \in \mathcal{T} \quad (8e)$$

$$\hat{v}_{i,t} - \hat{v}_{j,t} = \frac{1}{1 - \varphi_{ij}} (r_{ij} \hat{p}_{ij,t} + x_{ij} \hat{q}_{ij,t}), \forall ij \in \mathcal{L}, \forall t \in \mathcal{T} \quad (8f)$$

The Lossy DistFlow formulation [16] is employed to approximate the loss terms in voltage magnitude drop calculations within the traditional DistFlow model, as shown in (8f). This approach linearizes the voltage calculations while preserving a degree of accuracy.

4) *Networks security constraints*: The maximum power flow limits and voltage magnitude limits are enforced by constraints (9a)–(9b).

$$-\bar{p}^l \leq \hat{p}_{ij,t} \leq \bar{p}^l, \forall ij \in \mathcal{L}, \forall t \in \mathcal{T} \quad (9a)$$

$$\underline{v} \leq \hat{v}_{i,t} \leq \bar{v}, \forall i \in \mathcal{N}, \forall t \in \mathcal{T} \quad (9b)$$

Given the uncertainties of RESs and load demands, integrating the economic dispatch plan with a recourse control stage enhances operational flexibility. Compared to a single-stage approach, this model allows for dynamic adjustments by making recourse decisions in response to real-time variations in uncertainties, and co-optimizes active and reactive power dispatch across different timescales, thereby minimizing the need for conservative strategies and ensuring system security against uncertain scenarios [7].

III. CONFIDENCE LEVEL-BASED DISTRIBUTIONALLY INFORMATION GAP DECISION FORMULATION

A. Deterministic Model

A compact matrix-vector form of the optimization model presented in Section II is provided below for subsequent reformulation purpose.

$$\begin{aligned} \min_{\mathbf{x}, \mathbf{y}} \quad & \Lambda(\mathbf{x}, \mathbf{y}, \tilde{\xi}) = \mathbf{c}^T \mathbf{x} + \mathbf{d}^T \mathbf{y} & (10a) \\ \text{s.t.} \quad & \mathbf{A}\mathbf{x} \leq \mathbf{b} & (10b) \\ & \mathbf{E}\mathbf{x} \leq \mathbf{F}\tilde{\xi} & (10c) \\ & \mathbf{G}\mathbf{x} + \mathbf{H}\mathbf{y} \leq \mathbf{0} & (10d) \\ & \mathbf{I}\mathbf{x} + \mathbf{J}\mathbf{y} \leq \mathbf{L}\tilde{\xi} & (10e) \\ & \mathbf{M}\mathbf{y} \leq \mathbf{g} & (10f) \end{aligned}$$

In the above deterministic formulation, the total operational cost is indicated by $\Lambda(\mathbf{x}, \mathbf{y}, \tilde{\xi})$, where \mathbf{x} refers to the first-stage decision variable including $[p_{i,t}^G, p_{i,t}^{B+}, p_{i,t}^{B-}, z_{i,t}]$, \mathbf{y} is the second-stage decision variable including $[\hat{p}_{i,t}^G, \hat{q}_{i,t}^G]$, and $\tilde{\xi} = \tilde{p}^L - \tilde{p}^{PV}$ denotes the uncertain vector related to load demands and renewable energy, which adopt their forecasted values in the deterministic model. The variable \mathbf{x} is constrained by (10b), corresponding to constraints (2)-(3), (4a) and (5). Constraint (10c) correlates \mathbf{x} with the forecasted value of uncertain vector $\tilde{\xi}$, corresponding to constraint (4b). Constraint (10d) builds the relationship between \mathbf{x} and \mathbf{y} , corresponding to constraint (7c). Constraint (10e) correlates \mathbf{x} and \mathbf{y} with the forecasted value of uncertain vector $\tilde{\xi}$, corresponding to constraints (8c)-(8e). Finally, the remaining constraints concerning \mathbf{y} is represented by (10f).

B. Information-Gap Decision Model

DNs face significant uncertainties associated with RESs and load demands, necessitating a framework for uncertainty management. IGDT offers a non-probabilistic, non-fuzzy alternative that effectively handles uncertainties without the need to predefine the uncertainty extent [10]. The commonly used envelope-bound modelling by IGDT is shown below:

$$\Psi(\tilde{\xi}, \delta) = \left\{ \xi \mid \left| (\xi - \tilde{\xi}) \right| / \tilde{\xi} \leq \delta, \delta \geq 0 \right\} \quad (11)$$

where the variable δ represents the uncertainty extent.

The uncertainty modelling $\Psi(\tilde{\xi}, \delta)$ highlights the gap between the forecasted values and unknown information. For a given $\tilde{\xi}$, an increasing δ enhances the risk-averse capability, leading to a more costly solution, as it requires more resources to ensure performance and reliability under uncertainty. A major achievement of IGDT is its risk-averse capability, which refers to the maximum uncertainty extent obtained by driving

the actual system performance towards the desired target. As Fig. 1(a) shows, IGDT maximizes the uncertainty extent (safe region) to enable robust operational strategies. This is particularly advantageous in the energy dispatch field when the clear performance targets, such as the operational cost, are set by the distribution system operators. Under the desired target, the risk-averse capability against uncertainties associated with RESs and load demands is maximized. Consequently, this paper applies IGDT to handle the uncertain parameters in (10), which thus can be reformulated as follows:

$$\begin{aligned} \max_{\mathbf{x}, \mathbf{y}} \quad & \delta & (12a) \\ \text{s.t.} \quad & \mathbf{A}\mathbf{x} \leq \mathbf{b} & (12b) \\ & \mathbf{E}\mathbf{x} \leq \mathbf{F}\tilde{\xi} & (12c) \\ & \mathbf{G}\mathbf{x} + \mathbf{H}\mathbf{y}(\xi) \leq \mathbf{0}, \forall \xi \in \Psi(\tilde{\xi}, \delta) & (12d) \\ & \mathbf{I}\mathbf{x} + \mathbf{J}\mathbf{y}(\xi) \leq \mathbf{L}\xi, \forall \xi \in \Psi(\tilde{\xi}, \delta) & (12e) \\ & \mathbf{M}\mathbf{y}(\xi) \leq \mathbf{g}, \forall \xi \in \Psi(\tilde{\xi}, \delta) & (12f) \\ & \bar{\Lambda} \leq (1 + \sigma)\Lambda_0 & (12g) \\ & \bar{\Lambda} = \max_{\xi \in \Psi(\tilde{\xi}, \delta)} \Lambda(\mathbf{x}, \mathbf{y}(\xi), \xi) & (12h) \\ & = \mathbf{c}^T \mathbf{x} + \max_{\xi \in \Psi(\tilde{\xi}, \delta)} \mathbf{d}^T \mathbf{y}(\xi) \end{aligned}$$

IGDT formulation in (12) is a two-level optimization model. At the upper level, the objective is to maximize the uncertainty extent while enforcing the constraints (12b)-(12g). The lower level is specified in (12g)-(12h), where σ represents the deviation factor that defines the acceptable degree of budget excess, and Λ_0 is the system performance under the expected scenario. Through this two-level framework, robust performance $\bar{\Lambda}$ is deliberately driven towards the desired budget $(1 + \sigma)\Lambda_0$, ultimately enabling the optimal uncertainty extent.

The above uncertainty modelling requires little information on uncertainties, and it is well-suited for uncertain parameters exhibiting symmetric features. As shown in Fig. 1(a), such uncertainty set can perfectly capture the scenarios most likely to occur. Uncertain parameters like renewable generation and load demands, however, typically do not follow a symmetric distribution [17]. As demonstrated in Fig. 1(b), this misalignment can result in issues such as some safe regions being overlooked where actual scenarios would have occurred with high probability. For instance, scenarios where low renewable generation and high load demand, while significantly deviating from expected values, are uncommon yet still possible and may be excluded from the uncertainty set. Should they occur, these scenarios can compromise DN's safe operation. Additionally, the safe regions can be unnecessarily large due to the inclusion of impossible scenarios, leading to conservatism.

C. Confidence Level Based Information Gap Decision Model

To mitigate the aforementioned drawbacks and better handle the asymmetric characteristics of uncertain parameters, we propose utilizing confidence level-driven uncertainty set instead of the real-value symmetric one. This approach trans-

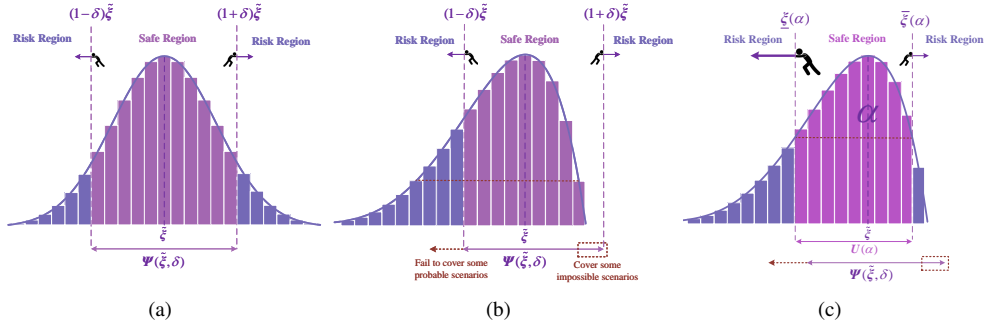


Figure 1. (a) The symmetric uncertainty set aligns perfectly with the shortest confidence interval of uncertain parameter characterized by symmetric probability density function; (b) For uncertain parameter with asymmetric characteristics, the symmetric uncertainty set no longer matches the shortest confidence interval; (c) The confidence level-driven uncertainty set captures the most probable uncertain scenarios, unlike the symmetric uncertainty set.

forms the uncertainty set into a suboptimization problem:

$$U(\alpha) = \left\{ \xi \mid \xi \in [\underline{\xi}(\alpha), \bar{\xi}(\alpha)] = \arg \min_{\underline{\xi}, \bar{\xi}} (\bar{\xi} - \underline{\xi}) : \right. \\ \left. F_{\xi}(\bar{\xi}) - F_{\xi}(\underline{\xi}) \geq \alpha, 0 \leq \alpha \leq 1 \right\} \quad (13)$$

where α represents the confidence level of the uncertainty set; $\bar{\xi}(\alpha)$ and $\underline{\xi}(\alpha)$ are the upper and lower bounds of the set, respectively, functions of α ; $F_{\xi}(\cdot)$ indicates the cumulative probability function (CDF) of ξ .

As illustrated in Fig. 1(c), the new uncertainty set covers the scenarios that are most likely to occur, which corresponds to the shortest confidence interval. This achieves the highest robustness with the least conservatism. Accordingly, the objective of IGDT is now to maximize α to allow the uncertainty set to capture as many of the probable uncertain scenarios as possible, significantly mitigating misalignment issues. The improved IGDT model can be transformed as follows:

$$\max_{x, y} \alpha \quad (14a)$$

$$\text{s.t. } Ax \leq b \quad (14b)$$

$$Ex \leq F\tilde{\xi} \quad (14c)$$

$$Gx + Hy(\xi) \leq 0, \forall \xi \in U(\alpha) \quad (14d)$$

$$Ix + Jy(\xi) \leq L\xi, \forall \xi \in U(\alpha) \quad (14e)$$

$$My(\xi) \leq g, \forall \xi \in U(\alpha) \quad (14f)$$

$$\bar{\Lambda} \leq (1 + \sigma)\Lambda_0 \quad (14g)$$

$$\bar{\Lambda} = \max_{\xi \in U(\alpha)} \Lambda(x, y(\xi), \xi) \\ = c^T x + \max_{\xi \in U(\alpha)} d^T y(\xi) \quad (14h)$$

By analysing the formulation in Section II, it is evident that the largest operational cost occurs when the electricity supply is at its peak, i.e., when renewable generation and load demands reach their bounds $\xi^*(\alpha) = \bar{p}^L(\alpha) - \underline{p}^{PV}(\alpha)$ within the uncertainty sets. Consequently, the two-level optimization model can be simplified into a single level one. Additionally, in standard IGDT, the use of a single variable δ becomes less practical when multiple uncertain parameters are involved. For the proposed model, however, we utilize probability to describe multiple uncertainties collectively, portraying the risk-averse capability in a probabilistic manner.

D. Construction of the Ambiguity Set

Introducing a confidence level α in (13) and (14) necessitates the CDFs, which may inherit the limitations associated

with SP method. To address this challenge, we draw inspiration from DRO and propose constructing ambiguity sets of CDFs. By fully utilizing available historical data and exploiting the implicit information it contains, the worst-case distribution can serve as a surrogate for the precise distribution.

Consider a dataset \mathcal{D} of a random variable ξ with K different values $\xi_k, k = 1, \dots, K$, arranged in an increasing order. Each value has an associated count n_k and an occurrence probability θ_k , respectively. A multinomial distribution can be used to model the uncertainty in these counts:

$$\Pr(N_1 = n_1, \dots, N_K = n_K) = \frac{n!}{\prod_{k=1}^K n_k!} \prod_{k=1}^K \theta_k^{n_k} \quad (15)$$

According to the Law of Large Numbers, parameter θ_k is estimated as $\theta_k = n_k/n$ as the total counts of sample $n \rightarrow \infty$. However, the limited size of historical dataset introduces inaccuracy into these probability estimates.

To quantify the imprecision in θ_k , the interval-valued probability is applied based on imprecise probability theory. IDM, an extension of the deterministic Dirichlet model, was proposed in [18] to estimate these intervals. IDM serves as a conjugate prior to the multinomial distribution, and utilizes a set of prior distributions rather than a single one, making it well-suited to model prior ignorance of θ_k , as shown in (16):

$$f(\theta) = \frac{\Gamma(\lambda)}{\prod_{k=1}^K \Gamma(\lambda \cdot r_k)} \prod_{k=1}^K \theta_k^{\lambda \cdot r_k - 1} \\ \forall r_k \in [0, 1], \sum_{k=1}^K r_k = 1 \quad (16)$$

where $\theta = [\theta_1, \dots, \theta_K]$, and $r = [r_1, \dots, r_K]$. r_k is the k th prior weight factor, λ indicates the total prior strength, and $\Gamma(\cdot)$ represents the Gamma function.

According to the property of PDF, the normalisation function $R(\lambda \cdot r_k)$ can be obtained:

$$R(\lambda \cdot r_k) = \frac{\prod_{k=1}^K \Gamma(\lambda \cdot r_k)}{\Gamma(\lambda)} = \int \prod_{k=1}^K \theta_k^{\lambda \cdot r_k - 1} \quad (17)$$

Within the Bayesian framework, the posterior distribution of θ is continually updated based on newly observed data, to consistently mitigate the prior ignorance. This dynamic adjustment is illustrated below.

$$\begin{aligned}
f(\boldsymbol{\theta} \mid \mathcal{D}) &= \frac{\prod_{k=1}^K \theta_k^{n_k} \cdot \frac{1}{R(\lambda \cdot r_k)} \prod_{k=1}^K \theta_k^{\lambda \cdot r_k - 1}}{\int \frac{1}{R(\lambda \cdot r_k)} \prod_{k=1}^K \theta_k^{\lambda \cdot r_k - 1} d\boldsymbol{\theta}} \\
&= \frac{1}{R(\lambda \cdot r_k + n_k)} \prod_{k=1}^K \theta_k^{\lambda \cdot r_k + n_k - 1}
\end{aligned} \quad (18)$$

Consequently, the imprecise parameter $\boldsymbol{\theta}$ of the multinomial distribution can be estimated by the expected values of (18). Considering the bounds of r_k , the probability intervals are computed as shown in (19). As more data accumulates, the associated intervals narrow, indicating greater precision [19].

$$\theta_k = \left[\frac{n_k}{n + \lambda}, \frac{n_k + \lambda}{n + \lambda} \right], k = 1, \dots, K \quad (19)$$

Since the CDF of ξ is defined as $F_\xi(x) = \Pr(\xi \leq x)$, it is easy to calculate the imprecise cumulative probability is $\left[\frac{n_k^*}{n + \lambda}, \frac{n_k^* + \lambda}{n + \lambda} \right]$, where n_k^* is the cumulative counts corresponding to $\xi \leq \xi_k$.

The interval estimated by IDM includes all possible probabilities corresponding to different priors. A probability interval with a quantitative confidence index, however, might be more suitable to construct the ambiguity set of RESs and load demands. The interval of cumulative probability can be estimated using credible index corresponding to IDM [18], [20]:

$$\begin{cases} \underline{\theta}_k = 0, \bar{\theta}_k = W^{-1}\left(\frac{1+\gamma}{2}\right), & n_k^* = 0 \\ \underline{\theta}_k = V^{-1}\left(\frac{1-\gamma}{2}\right), \bar{\theta}_k = W^{-1}\left(\frac{1+\gamma}{2}\right), & 0 \leq n_k^* \leq n \\ \underline{\theta}_k = V^{-1}\left(\frac{1-\gamma}{2}\right), \bar{\theta}_k = 1, & n_k^* = n \end{cases} \quad (20)$$

where γ is the confidence index to estimate the probability interval. $V(\cdot)$ and $W(\cdot)$ are the CDFs of Beta distribution, i.e., Beta($n_k^*, s + n - n_k^*$) and Beta($s + n_k^*, n - n_k^*$), respectively.

To make the CDFs smoother due to the limited sample points in \mathcal{D} , a simple interpolation method is applied to obtain the probability intervals at non-sample points [9]. The interval-valued probability at non-sample points can be expressed as:

$$\begin{cases} \Pr(\xi \leq \xi_\kappa) = \underline{\theta}_\kappa, & \kappa \in [k, k+1) \\ \Pr(\xi \leq \xi_\kappa) = \bar{\theta}_{\kappa+1}, & \kappa \in (k, k+1] \end{cases} \quad (21)$$

where κ indicates the non-sample points between two sample points k and $k+1$.

Finally, the ambiguity set is constructed by connecting the upper and lower bounds of these probability intervals, which can be constructed as:

$$\mathcal{A} = \{F_\xi \mid F_\xi(x) \in [\underline{\Pr}(\xi \leq x), \bar{\Pr}(\xi \leq x)]\} \quad (22)$$

E. Selection of the Worst-case Distribution

After calculating the accumulative counts of different values of solar power p^{PV} , for example, (20) and (21) can be used to calculate the interval-valued cumulative probability and then construct the ambiguity set \mathcal{A}_{PV} , as depicted in Fig. 2.

When actual solar power disturbances remain within the safe region obtained by IGDT method, the total operational cost is constrained within the preset budget while ensuring network security. Conversely, disturbances that extend beyond this region into the risk area may require additional actions

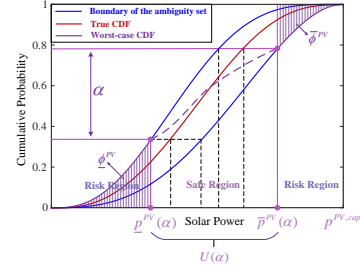


Figure 2. Ambiguity set of solar power. Given α , the optimal uncertainty set over the worst-case distribution (illustrated with purple dots) is the longest compared to those derived from alternative distributions (represented by black dots). This suggests that alternative distributions are not the worst-case distribution which necessitates consideration of a wider fluctuation range, resulting in higher operational costs.

to address unexpected conditions, or even potentially compromise the network security.

To quantify the associated operational risk, the indicator CVaR is utilized [9]. It is assumed that the upside risk is caused by excessive solar power, whereas the downside risk is due to insufficient solar power.

The downside risk (ϕ^{PV}) is quantified as follows:

$$\begin{aligned}
\underline{\phi}^{PV} &= \int_0^{\underline{p}^{PV}} (\underline{p}^{PV} - x) f_{p^{PV}}(x) dx \\
&= \int_0^{\underline{p}^{PV}} F_{p^{PV}}(x) dx
\end{aligned} \quad (23)$$

Considering the ambiguity in CDFs, the maximal downside risk is:

$$\max_{F_{p^{PV}} \in \mathcal{A}_{PV}} \underline{\phi}^{PV} = \max_{F_{p^{PV}} \in \mathcal{A}_{PV}} \int_0^{\underline{p}^{PV}} F_{p^{PV}}(x) dx \quad (24)$$

As illustrated in Fig. 2, the maximal downside risk equals to the shaded area between $F_{p^{PV}}$ and the interval $[0, \underline{p}^{PV}]$. Obviously, $\bar{F}_{p^{PV}}$ leads to the highest downside risk, thus representing the worst-case distribution when the actual solar power exceeds its left boundary of the uncertainty set. Similarly, $\underline{F}_{p^{PV}}$ achieves the highest upside risk, representing the worst-case distribution when the real solar power exceeds the right boundary of the uncertainty set. The worst-case distribution of solar power $F_{p^{PV}}^*(\cdot)$ can be expressed as:

$$F_{p^{PV}}^*(x) = \begin{cases} \bar{F}_{p^{PV}}(x), & p^{PV} \leq \underline{p}^{PV} \\ \underline{F}_{p^{PV}}(x), & p^{PV} \geq \bar{p}^{PV} \end{cases} \quad (25)$$

With the construction of the ambiguity sets and the selection of the worst-case distribution pairs, the confidence level-driven uncertainty set in (13), which was originally based on precise CDFs, is now replaced by the one constructed using ambiguity sets, as (26) shows.

$$\begin{aligned}
U(\alpha) &= \left\{ \xi \mid \xi \in [\underline{\xi}(\alpha), \bar{\xi}(\alpha)] = \arg \min_{\bar{\xi}, \underline{\xi}} (\bar{\xi} - \underline{\xi}) : \right. \\
&\quad \left. \underline{F}_\xi(\bar{\xi}) - \bar{F}_\xi(\underline{\xi}) \geq \alpha, 0 \leq \alpha \leq 1 \mid \underline{F}_\xi, \bar{F}_\xi \in \mathcal{A} \right\} \quad (26)
\end{aligned}$$

IV. SOLUTION METHODOLOGY

This section presents the methodology to solve the proposed optimization framework shown in (14) and (26). A piecewise

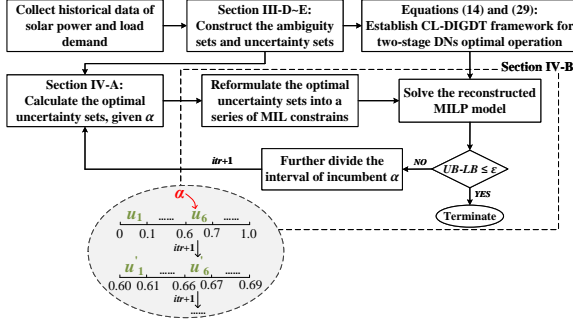


Figure 3. Flowchart of the solution methodology.

linearization approximation (PLA) method is utilized to linearize the CDFs that lack closed-form expressions, thereby facilitating the obtaining of the optimal uncertainty set offline. The optimization formulation is thus transformed into a mixed integer linear programming (MILP) model. An iterative method is introduced to determine the upper and lower bounds of the optimal α until the required accuracy is achieved. Overall, the proposed methodology is outlined in Fig. 3.

A. Calculation of Optimal Uncertainty Set

Explicitly expressing the uncertainty set in (26) is challenging, as the suboptimization problem lacks closed-form distributions which are constructed by a series of discrete points, and thus deriving the optimality conditions is inapplicable. However, leveraging the structure of the proposed framework, we devise a method to calculate the optimal uncertainty set offline, and subsequently integrate it into the original model.

Assume the optimal objective value is α in (26). The PLA method [21] enables the approximated transformation of (26) into a MILP, thereby facilitating the derivation of the optimal uncertainty set. Again, we take solar power as an example.

Step 1: The range of p_t^{PV} is segmented into equal intervals marked by a series of breakpoints $o_{t,s}, s = 1, \dots, S$. Each interval is associated with a binary variable $a_{t,s}$ to determine whether the actual lower bound p_t^{PV} , for instance, falls within this interval, which can be expressed as:

$$\begin{cases} p_t^{PV} = \sum_{s=1}^{S-1} p_{t,s}^{PV} \\ \sum_{s=1}^{S-1} a_{t,s} = 1 \\ a_{t,s} o_{t,s} \leq p_{t,s}^{PV} \leq a_{t,s} o_{t,s+1} \end{cases} \quad (27)$$

Step 2: The cumulative probability of $p_{t,s}^{PV}$ can be obtained as $F_{p_t^{PV}}(o_{t,s})$ when it is exactly equal to the breakpoint, i.e., $p_{t,s}^{PV} = o_{t,s}$.

Step 3: The general expression of worst-case cumulative probability of p_t^{PV} can be linearized as:

$$\begin{aligned} \bar{F}_{p_t^{PV}}(p_t^{PV}) &= \int_0^{o_{t,s}} \bar{f}_{p_t^{PV}}(x) dx + (p_{t,s}^{PV} - o_{t,s}) \bar{f}_{p_t^{PV}}(o_{t,s}) \\ &= \sum_{s=1}^{S-1} \omega_{t,s} p_{t,s}^{PV} + \beta_{t,s} a_{t,s} \end{aligned} \quad (28)$$

where

$$\begin{aligned} \omega_{t,s} &= \frac{\bar{F}_{p_t^{PV}}(o_{t,s+1}) - \bar{F}_{p_t^{PV}}(o_{t,s})}{o_{t,s+1} - o_{t,s}} \\ \beta_{t,s} &= -\frac{\bar{F}_{p_t^{PV}}(o_{t,s+1}) - \bar{F}_{p_t^{PV}}(o_{t,s})}{o_{t,s+1} - o_{t,s}} o_{t,s} + \bar{F}_{p_t^{PV}}(o_{t,s}) \end{aligned}$$

For this approach, only the cumulative probabilities at breakpoints are necessary. Likewise, the worst-case distributions $\underline{F}_{p_t^{PV}}(\bar{p}_t^{PV})$, $\bar{F}_{p_t^L}(\underline{p}_t^L)$, and $\underline{F}_{p_t^L}(\bar{p}_t^L)$ can also be transformed into mixed integer linear equations. Consequently, the suboptimization problem of calculating optimal uncertainty set becomes a MILP, which can be addressed using a commercial solver, provided a specific α is given.

B. Iteration Solving Procedure

The optimal uncertainty set depends on the optimal α , which remains unknown until the problem is solved. Fortunately, given the range of the objective function is from 0 to 1, the structured nature of the optimization problem can be exploited to allow for an iterative method, where a larger objective value will lead to a higher worst-case cost. The solving procedure is shown in Fig. 3, and the details are as follows.

Step 1: The initial step is set as $itr = 1$. Assume that α takes values from ten equal intervals separated by discrete points, $0, 0.1, \dots, 1.0$. Binary variables $u_m, m = 1, \dots, 10$ are utilized to determine which interval α falls into, as shown below.

$$\begin{cases} \alpha = \sum_{m=1}^{10} \alpha_m \\ \underline{\alpha}_m^{(itr)} \cdot u_m \leq \alpha_m \leq \bar{\alpha}_m^{(itr)} \cdot u_m, \forall m \\ \sum_{m=1}^{10} u_m = 1 \end{cases} \quad (29)$$

where

$$\begin{aligned} \underline{\alpha}_m^{(itr)} &= 10^{-itr} (m-1) \\ \bar{\alpha}_m^{(itr)} &= 10^{-itr} m \end{aligned} \quad (30)$$

Step 2: Given the values of each known $\underline{\alpha}_m$, the corresponding optimal uncertainty set of solar power and load demands can be obtained offline by using the approach in Section IV-A, i.e., $U_t^{PV}(\underline{\alpha}_m) = [p_t^{PV}(\underline{\alpha}_m), \bar{p}_t^{PV}(\underline{\alpha}_m)]$ and $U_t^L(\underline{\alpha}_m) = [p_t^L(\underline{\alpha}_m), \bar{p}_t^L(\underline{\alpha}_m)], \forall t, \forall m = m \cup \{11\}$.

Step 3: The optimal uncertainty sets corresponding to different $\underline{\alpha}_m$ are formulated as a series of constraints and then embed into the original optimization problem. The big M technique is utilized to determine which set of constraints associated with the optimal α are active, as shown below.

$$\begin{cases} p_t^{PV}(\underline{\alpha}_m) - M(1 - u_m) \leq p_t^{PV} \\ \leq \bar{p}_t^{PV}(\underline{\alpha}_m) + M(1 - u_m), \\ p_t^L(\underline{\alpha}_m) - M(1 - u_m) \leq p_t^L \\ \leq \bar{p}_t^L(\underline{\alpha}_m) + M(1 - u_m) \end{cases} \quad (31)$$

Step 4: The original problem now consists of a series of mixed integer linear constraints, transforming the entire optimization problem into a MILP, which can be solved directly by commercial solvers. Since α assumes taking value from only ten intervals, the incumbent solution may lack precision. The boundaries of the interval which the incumbent α falls into $[\underline{\alpha}^{(itr*)}, \bar{\alpha}^{(itr*)}]$ serve as the lower bound LB and upper bound UB of the optimal α^* , respectively. To obtain more

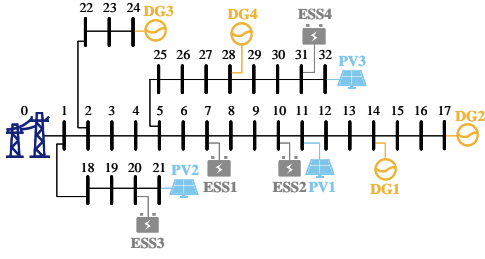


Figure 4. Modified IEEE 33-bus system.

Table I
DGs INFORMATION

Label	\bar{p}^G (kW)	\underline{p}^G (kW)	RU (kW)	RD (kW)	\bar{q}^G (kW)	\underline{q}^G (kW)	c (\\$)
DG1	600	100	100	100	500	-400	4.0
DG2	400	100	90	90	300	-200	3.5
DG3	250	80	60	60	200	-150	2.5
DG4	50	10	15	15	40	-25	2.0

accurate result, we further divide the obtained interval into ten updated smaller intervals, and set the iteration itr to $itr + 1$.

$$\begin{cases} \alpha = \sum_{m=1}^{10} \alpha_m \\ (\underline{\alpha}^{(itr^*)} + \underline{\alpha}_m^{(itr)}) \cdot u'_m \leq \alpha_m \leq (\bar{\alpha}^{(itr^*)} + \bar{\alpha}_m^{(itr)}) \cdot u'_m, \forall m \\ \sum_{m=1}^{10} u'_m = 1 \end{cases} \quad (32)$$

Given ten new discrete values, the corresponding optimal uncertainty set can be calculated offline again. Embed them into the original optimization problem and resolve it, so the new information can be updated as $UB = \bar{\alpha}^{(itr^*)}$, $LB = \underline{\alpha}^{(itr^*)}$, and $itr = itr + 1$.

Step 5: Further segmentation of α into smaller intervals is possible if $UB - LB \leq \epsilon$ does not satisfy, where ϵ indicates the specified accuracy. *Step 4* with smaller resolution will be repeated, or the optimal solution is assumed to be reached.

V. CASE STUDY AND DISCUSSION

The proposed framework was tested on modified IEEE 33-bus system, as illustrated in Fig. 4. The system data is available in [22], and the data for DGs and ESSs is given in Table I and Table II, respectively. All simulations were implemented on a 64-bit PC with a 3.00-GHz CPU and 16 GB RAM using Gurobi API in PyCharm. The time period were set to one day, with a resolution of one hour. Solar power and load demand for each bus are deemed to be uncertain sources. Approximately one year of historical data were used to construct the ambiguity sets. The confidence index γ and total prior strength λ for IDM are set to 0.95 and 1 [20], respectively.

A. Optimal Operation Results for Distribution Networks

To illustrate the basic results of the proposed method, DT- and IGDT-based approaches are chosen as benchmarks. The deviation factor σ is set as 30%, and all other parameters remain consistent. The optimal cost of DT is 216,773\$, which determines the desired budget for IGDT and CL-DIGDT. The optimal uncertainty extent obtained by IGDT is 0.183. This result indicates that, by implementing the optimal operational scheme, whenever the actual solar power and load demands fall within the safe regions where deviations are within 18.3% of their predicted values, system safety is ensured and the

Table II
ESSs INFORMATION

Label	\bar{p}^B (kW)	\underline{p}^B (kW)	\bar{e} (kW)	\underline{e} (kW)	η_B
ESS1	120	120	600	120	0.9
ESS2	40	40	200	40	0.9
ESS3	60	60	300	60	0.9
ESS4	80	80	400	80	0.9

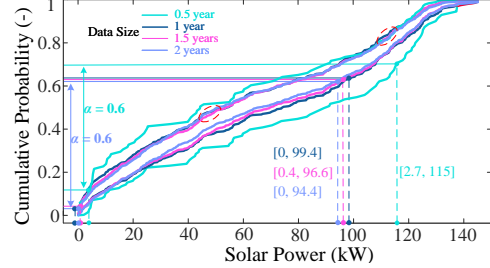


Figure 5. Ambiguity sets of solar power with different data size.

total operational cost will remain within the preset budget, or otherwise no guarantees can be made. For CL-DIGDT, the optimal probability is 0.665. The same explanation applies, but the safe regions are defined by the shortest confidence intervals corresponding to this probability.

B. Ambiguity Sets within Proposed Framework

According to the previous research in [19] and [9], as the sample size consistently increases, the ambiguity set shrinks and the worst-case distribution is expected to be converged towards the true distribution. Consequently, the optimal uncertainty sets obtained should become progressively shorter, thereby reducing conservatism. Fig. 5 illustrates the ambiguity sets of solar power constructed using varying sizes of historical data and the optimal uncertainty set corresponding to each size, given $\alpha = 0.6$. Interestingly, as the data size increases, the ambiguity set enlarges slightly in some areas (e.g., those highlighted in ellipses), and the optimal uncertainty sets do not completely envelop the one obtained from a larger data size, which appears to contradict the theory to some extent. Upon further analysis, two reasons for this contradiction emerge.

Firstly, the distribution's shape can initially be rough when the data size is small. This explains the significant change in the shape of the ambiguity set initially, but eventually stabilizing and approaching its real shape as more data is incorporated. Secondly, the initial sample size may be insufficient, and thus the limited discrete points inadequately represent the confidence level of 0.6, causing a deviation in the uncertainty set. It is suggested that with a sufficiently large dataset, the actual distribution and the optimal uncertainty set will be accurately captured, thereby reducing conservatism and aligning with theoretical expectations.

C. Optimal Uncertainty Sets of Different Approaches

As shown in Fig. 6(a), the uncertainty set (safe region) obtained by CL-DIGDT method is notably larger than that obtained by IGDT. Though larger uncertainty sets can lead to higher costs, it is probabilistically worthwhile to guarantee robustness at the expense of economic performance. It is because the safe region of the proposed method nearly (considering ambiguity) encompasses the scenarios with the highest

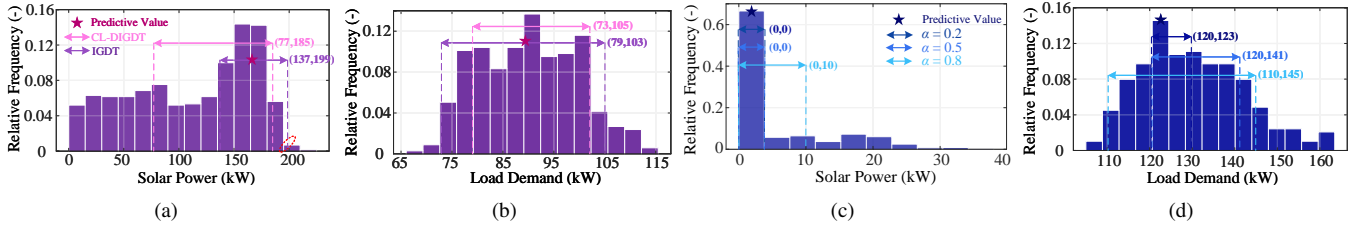


Figure 6. Optimal uncertainty sets. (a) Solar power for time period 11:00-12:00; (b) Load demand at node 20 for time period 1:00-2:00; (c) Solar power for time period 8:00-9:00; (d) Load demand at node 21 for time period 13:00-14:00.

probability of occurrence, whereas the uncertainty set obtained by IGDT is centered around its predictive value and includes some unnecessary scenarios (those highlighted in ellipse).

In contrast, Fig. 6(b) illustrates the shorter uncertainty set obtained by CL-DIGDT than IGDT. In this case, the most probable scenarios are relatively centered around its predictive value. To probabilistically ensure economic performance, scenarios with low probabilities of occurrence are excluded from the safe region to shorten the uncertainty set. It is also worth noting that the differences between the uncertainty sets obtained by the two approaches are reduced compared to Fig. 6(a), as the asymmetry of the distribution is significantly mitigated. It is reasonable to infer that if the distribution exhibits symmetric characteristics, such as a Gaussian distribution, the difference in uncertainty set will diminish further, potentially becoming nearly identical. Therefore, the trade-off between economic performance (smaller uncertainty set) and robustness (larger uncertainty set) can be guaranteed in a probabilistic manner, depending on the feature of the data.

To further explore the superiority of the proposed uncertainty modelling, the optimal intervals under different α were examined. Fig. 6(c) shows that interval remains stable even though α increases from 0.2 to 0.5. While α reaches 0.8, this interval changes noticeably. The nonlinear expansion of the interval occurs since the solar power is predominantly centered around zero. For load demands without any distribution pattern shown in Fig. 6(d), the interval also expands nonlinearly rather than linearly as IGDT method. This indicates nonlinear robustness is considered in the proposed method.

D. Post-Evaluation of Different Approaches

The ‘here-and-now’ decision \mathbf{x} is robustly optimized and serves as the final scheme, while the ‘wait-and-see’ decisions \mathbf{y} can dynamically adjust in response to the realization of the uncertain scenarios. To assess the risk-averse capability of CL-DIGDT solution, post-evaluation is conducted on \mathbf{x} , using 50 randomly selected scenarios which did not include in the ambiguity sets. The performance metric is the expected project budget (EPB) [23] defined in (33), and the reliability of the solutions, which refers to the percentage of feasible solutions.

$$EPB = \mathbf{c}^T \mathbf{x} + \frac{1}{NF} \sum_{n=1}^{NF} \mathbf{d}^T \mathbf{y}_n \quad (33)$$

where NF represents the number of common feasible solutions shared by different approaches.

As shown in Fig. 7, the DT method incurs the highest EPB and yields the lowest reliability. The optimal \mathbf{x}^* contributes

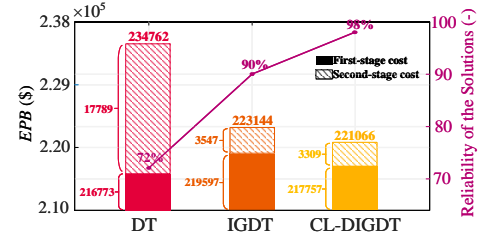


Figure 7. Results of post-evaluation obtained by different approaches.

to the lowest first-stage cost because it is just optimized under a single expected scenario. Without considering any potential uncertainty, the solution lacks risk-averse capability and requires substantial adjustments to compensate for the impact of the uncertain scenarios that were not taken into consideration during the decision process, thus resulting in an extremely high second-stage cost and the lowest reliability. In contrast, the robustness of the IGDT solution is achieved by investing 30% more budget. By considering possible uncertain scenarios, higher first-stage cost is incurred but a significant reduction in the second-stage cost and a substantial increase in the reliability of the solutions are expected.

The CL-DIGDT approach further reduces EPB and enhances reliability by accounting for the asymmetric feature of uncertainties and leveraging implicit patterns within the historical data to optimize \mathbf{x} . Compared to the IGDT, the proposed approach reduced the first-stage cost by 0.84% and the second-stage average cost by 6.7%. As discussed in Section V-C, unnecessary robustness is avoided (which reduces the cost) while necessary robustness is maintained (which increases the cost). These two cases offset each other, so as to ensure the best trade-off between risk-averse capability and economic performance (which can be demonstrated in Fig. 7 by the lower first-stage cost still contributing to lower second-stage cost and higher reliability). This explains why the improvement in economic performance, relative to the total operational costs, is relatively modest, while the reliability of the solutions is fairly enhanced by 8% compared to IGDT. Consequently, the proposed approach achieves a more robust and statistically optimized solution. Furthermore, it is safe to suggest the superiority will be more pronounced if the asymmetric characteristics of uncertainties become more severe.

E. Sensitivity Analysis

The impact of the deviation factor σ on the objective functions of IGDT and CL-DIGDT methods is analyzed. Fig. 8 illustrates their corresponding values of δ and α , which indicate the risk-averse capability of the optimal solutions with

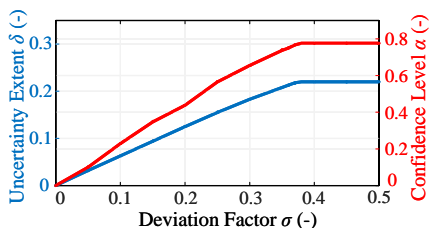


Figure 8. Sensitivity analysis of deviation factor.

Table III
ACCURACY OF THE OPTIMAL SOLUTIONS

Iterations	Incumbent α	Range of α^*	EPB (\$)	Reliability
1	0.6	[0.60,0.69]	223453	96%
2	0.66	[0.660,0.669]	223434	98%
3	0.665	[0.6650,0.6659]	223421	98%
4	0.6651	[0.66510,0.66519]	223404	98%

regards to the varying σ . The risk-averse capability increases linearly as more budget is allocated, meaning that both approaches provide higher robustness at the expense of economical performance. However, as discussed in Section V-C, the uncertainty sets of CL-DIGDT increases nonlinearly even with a linear increase in α , unlike the linear response of IGDT method. Notably, when σ approaches around 0.4, the risk-averse capability plateaus for both approaches, signifying that the maximum level of robustness has been reached due to the limited availability of dispatchable resources within the DNs. This suggests that the risk-averse capability may further enhance if additional dispatchable resources are considered.

F. Accuracy of the Optimal Solutions

The iteration method in Section IV is to determine the upper and lower bounds of the objective function in (14a). To test the validity of the proposed method, different accuracy requirements were tested. As iterations progress, the incumbent α becomes more accurate, as Table III shows, thus leading to increasingly refined confidence level-driven uncertainty sets. Additionally, as the accuracy of α improves, the EPB decreases and the reliability of the solutions is enhanced. This indicates that the incumbent solution progressively moves towards the optimal α^* . Once the preset accuracy threshold is met, the incumbent solution is considered sufficiently optimal.

VI. CONCLUSION

This paper proposes a CL-DIGDT framework for the two-stage optimal operation of distribution networks. The proposed method incorporates a confidence level to capture the asymmetric characteristics of uncertainties and to maximize the risk-averse capability of the operational scheme in a probabilistic manner. The IDM is used to construct the ambiguity sets for solar power and load demands, thereby reducing the dependence on precise CDFs. An iterative method is introduced to solve the proposed optimization model.

The results illustrate that, as data size increases, the ambiguity sets and confidence level-driven uncertainty sets become more accurate. As additional budget is allocated, the risk-averse capability of the solution obtained by CL-DIGDT increases linearly but eventually plateaus due to the limited dispatchable resources, whereas the corresponding uncertainty

sets expand nonlinearly. Post-evaluation demonstrates the operational scheme obtained by the proposed method achieves the best trade-off between economic performance and robustness, with a reduction in the first-stage cost by 0.84% and the second-stage average cost by 6.7%, and the reliability of the solution increased significantly by 8%. The effectiveness of the proposed solution methodology is proved by less EPB and higher reliability with the increased iterations.

REFERENCES

- [1] J. Hu, X. Liu, M. Shahidehpour, and S. Xia, "Optimal operation of energy hubs with large-scale distributed energy resources for distribution network congestion management," *IEEE Trans. Sustain. Energy*, vol. 12, no. 3, pp. 1755–1765, 2021.
- [2] Z. Wu, P. Zeng, X.-P. Zhang, and Q. Zhou, "A solution to the chance-constrained two-stage stochastic program for unit commitment with wind energy integration," *IEEE Trans. Power Syst.*, vol. 31, no. 6, pp. 4185–4196, 2016.
- [3] Y. Liu and N.-K. C. Nair, "A two-stage stochastic dynamic economic dispatch model considering wind uncertainty," *IEEE Trans. Sustain. Energy*, vol. 7, no. 2, pp. 819–829, 2016.
- [4] S. Chen, C. Wang, and Z. Zhang, "Multitime scale active and reactive power coordinated optimal dispatch in active distribution network considering multiple correlation of renewable energy sources," *IEEE Trans. Ind. Appl.*, vol. 57, no. 6, pp. 5614–5625, 2021.
- [5] Y. Zhang, X. Ai, J. Wen, J. Fang, and H. He, "Data-adaptive robust optimization method for the economic dispatch of active distribution networks," *IEEE Trans. Smart Grid*, vol. 10, no. 4, pp. 3791–3800, 2019.
- [6] C. Lu, N. Gu, W. Jiang, and C. Wu, "Sample-adaptive robust economic dispatch with statistically feasible guarantees," *IEEE Trans. Power Syst.*, vol. 39, no. 1, pp. 779–793, 2024.
- [7] Y. Yang and W. Wu, "A distributionally robust optimization model for real-time power dispatch in distribution networks," *IEEE Trans. Smart Grid*, vol. 10, no. 4, pp. 3743–3752, 2019.
- [8] J. Liu, Y. Chen, C. Duan, J. Lin, and J. Lyu, "Distributionally robust optimal reactive power dispatch with wasserstein distance in active distribution network," *J. Mod. Power Syst. Clean Energy*, vol. 8, no. 3, pp. 426–436, 2020.
- [9] P. Li, M. Yang, and Q. Wu, "Confidence interval based distributionally robust real-time economic dispatch approach considering wind power accommodation risk," *IEEE Trans. Sustain. Energy*, vol. 12, no. 1, pp. 58–69, 2021.
- [10] Y. Ben-Haim, *Info-gap decision theory: decisions under severe uncertainty*. Elsevier, 2006.
- [11] A. O'Connell, A. Soroudi, and A. Keane, "Distribution network operation under uncertainty using information gap decision theory," *IEEE Trans. Smart Grid*, vol. 9, no. 3, pp. 1848–1858, 2018.
- [12] N. Rezaei, A. Ahmadi, A. H. Khazali, and J. M. Guerrero, "Energy and frequency hierarchical management system using information gap decision theory for islanded microgrids," *IEEE Trans. Ind. Electron.*, vol. 65, no. 10, pp. 7921–7932, 2018.
- [13] M. Izadi, S. Hossein Hosseini, S. Dehghan, A. Fakharian, and N. Amjadi, "Resiliency-oriented operation of distribution networks under unexpected wildfires using multi-horizon information-gap decision theory," *Appl. Energy*, vol. 334, p. 120536, 2023.
- [14] M. Ahmadigorji, N. Amjadi, and S. Dehghan, "A robust model for multi-year distribution network reinforcement planning based on information-gap decision theory," *IEEE Trans. Power Syst.*, vol. 33, no. 2, pp. 1339–1351, 2018.
- [15] X. Dai, Y. Li, K. Zhang, and W. Feng, "A robust offering strategy for wind producers considering uncertainties of demand response and wind power," *Appl. Energy*, vol. 279, p. 115742, 2020.
- [16] E. Schweitzer, S. Saha, A. Scaglione, N. G. Johnson, and D. Arnold, "Lossy distflow formulation for single and multiphase radial feeders," *IEEE Trans. Power Syst.*, vol. 35, no. 3, pp. 1758–1768, 2020.
- [17] M. Anvari, E. Proedrou, B. Schäfer, C. Beck, H. Kantz, and M. Timme, "Data-driven load profiles and the dynamics of residential electricity consumption," *Nat. commun.*, vol. 13, no. 1, p. 4593, 2022.
- [18] P. Walley, "Inferences from multinomial data: learning about a bag of marbles," *J. R. Stat. Soc., B: Stat. Methodol.*, vol. 58, no. 1, pp. 3–34, 1996.
- [19] J.-M. Bernard, "An introduction to the imprecise dirichlet model for multinomial data," *Int. J. Approx. Reason.*, vol. 39, no. 2-3, pp. 123–150, 2005.

- [20] M. Yang, J. Wang, H. Diao, J. Qi, and X. Han, "Interval estimation for conditional failure rates of transmission lines with limited samples," *IEEE Trans Smart Grid*, vol. 9, no. 4, pp. 2752–2763, 2016.
- [21] M. Q. Wang, H. B. Gooi, S. X. Chen, and S. Lu, "A mixed integer quadratic programming for dynamic economic dispatch with valve point effect," *IEEE Trans. Power Syst.*, vol. 29, no. 5, pp. 2097–2106, 2014.
- [22] M. Baran and F. Wu, "Network reconfiguration in distribution systems for loss reduction and load balancing," *IEEE Trans. Power Deliv.*, vol. 4, no. 2, pp. 1401–1407, 1989.
- [23] X. Cao, J. Wang, and B. Zeng, "A chance constrained information-gap decision model for multi-period microgrid planning," *IEEE Trans. Power Syst.*, vol. 33, no. 3, pp. 2684–2695, 2018.